J. Fluid Mech. (2011), *vol.* 685, *pp.* 532–542.
doi:10.1017/jfm.2011.338

Frontal instabilities and waves in a differentially rotating fluid

J.-B. Flór[1]†, H. Scolan[1] and J. Gula[2]‡

[1] Laboratoire des Écoulements Géophysiques et Industriels, CNRS and Université de Grenoble, BP 53, 38041 Grenoble, France

[2] Laboratoire de Metéorologie Dynamique, rue Lhomond 75005, Paris, France

(Received 25 February 2011; revised 28 June 2011; accepted 3 August 2011; first published online 22 September 2011)

We present an experimental investigation of the stability of a baroclinic front in a rotating two-layer salt-stratified fluid. A front is generated by the spin-up of a differentially rotating lid at the fluid surface. In the parameter space set by rotational Froude number, F, dissipation number, d (i.e. the ratio between disk rotation time and Ekman spin-down time) and flow Rossby number, a new instability is observed that occurs for Burger numbers larger than the critical Burger number for baroclinic instability. This instability has a much smaller wavelength than the baroclinic instability, and saturates at a relatively small amplitude. The experimental results for the instability regime and the phase speed show overall a reasonable agreement with the numerical results of Gula, Zeitlin & Plougonven (*J. Fluid Mech.*, vol. 638, 2009, pp. 27–47), suggesting that this instability is the Rossby–Kelvin instability that is due to the resonance between Rossby and Kelvin waves. Comparison with the results of Williams, Haines & Read (*J. Fluid Mech.*, vol. 528, 2005, pp. 1–22) and Hart (*Geophys. Fluid Dyn.*, vol. 3, 1972, pp. 181–209) for immiscible fluid layers in a small experimental configuration shows continuity in stability regimes in (F, d) space, but the baroclinic instability occurs at a higher Burger number than predicted according to linear theory. Small-scale perturbations are observed in almost all regimes, either locally or globally. Their non-zero phase speed with respect to the mean flow, cusped-shaped appearance in the density field and the high values of the Richardson number for the observed wavelengths suggest that these perturbations are in many cases due to Hölmböe instability.

Key words: baroclinic flows, quasi-geostrophic flows, waves in rotating fluids

1. Introduction

Fronts occur in the atmosphere and oceans and are marked by a sharp transition in density and shear. In separating energy, mass and momentum, their dynamics are relevant for large-scale circulation and climate models. Since the work of Charney (1947) and Eady (1949) on baroclinic instability, the dynamics of frontal instability has attracted a large number of researchers (see e.g. the review by Hart 1979 and

† Email address for correspondence: flor@hmg.inpg.fr

‡ Present address: University of Toronto, Department of Physics, Toronto, Canada

the textbook of Pedlosky 1987). Most of these studies concern instability in quasi-geostrophic flows. In the present study we focus on ageostrophic effects.

In exploring ageostrophic instability, Sakai (1989) investigated new resonant combinations between gravity waves and Rossby waves for a front in a two-layer fluid. For waves moving in the upper and lower layers in opposite directions, resonance can be expected when the Doppler-shifted frequencies of the waves match. For instance, baroclinic instability can then be explained as a resonance between the Rossby waves in each layer. With this approach, Sakai (1989) found the instability for the resonance between Rossby and Kelvin waves, further called the Rossby–Kelvin instability (below briefly RK). In continuing this work, Gula, Plougonven & Zeitlin (2009*a*) and Gula, Zeitlin & Plougonven (2009*b*) considered different geometries (i.e. for a channel Gula *et al.* 2009*a* and annular flow Gula *et al.* 2009*b*), included new regions of instability and also considered numerically the effect of continuous stratification.

In the laboratory, frontal instability has been investigated in particular in differentially rotating fluids or fluids that are differentially heated to create a lateral density gradient. By the geostrophic balance, either of these forcing mechanisms leads to the formation of a front in density and shear, as shown in differential spin-up experiments and heated annulus experiments (see the review by Hart 1979). Baroclinic instability of fronts has also been considered in the context of spin-up of stratified fluids (e.g. Spence, Foster & Davies 1992; Flór *et al.* 2004). We focus on a baroclinic front generated in a differentially rotating fluid as studied by Hart (1972), Lovegrove, Read & Richards (2000) and Williams, Haines & Read (2005) (further referred to as WHR), but in a differentially rotating annulus which is eight times larger than that in WHR, and filled with a miscible two-layer stratified fluid (see Flór 2007), thus allowing for mixing and diffusion between the layers, and no viscous dissipative effects as may occur between immiscible fluids of different viscosity.

Our attention is focused on the experimental observation of the RK instability, recently investigated numerically by Gula *et al.* (2009*a*,*b*). They showed that this instability converts 2/3 of its kinetic energy into potential energy and 1/3 into small-scale instabilities. By contrast, the baroclinic instability converts approximately 25 times more potential energy into kinetic energy. The RK instability has growth rates that are comparable to, or larger than, that of the baroclinic instability, especially at sharp interfaces. With increasing interface thickness, modes are found to be trapped at the interface and weaker growth rates are found. In contrast to baroclinic instability, the RK instability saturates at an early stage. Small-scale instabilities appear in the largest frontal excursions of the RK waves and are of Kelvin–Helmholtz (KH) type. The numerical simulations of Gula *et al.* (2009*a*) show that for Reynolds numbers less than 2000, the diffusion of the front precedes the development of the RK instability. Small-scale motions significantly moderate the mean flow, making the coupling between Rossby and Kelvin waves less likely to occur in small-scale flows for weak Reynolds numbers.

The paper is organized as follows. In the next section, the experimental setup is presented. The observations of the different instability regimes in the (F, d) parameter space are discussed in § 3, followed in § 4 by a comparison of the RK instability of Sakai (1989) with the results found by Gula *et al.* (2009*b*). In § 5, we consider wave observations in the context of Hölmböe instability, Kelvin–Helmholtz instability and spontaneously emitted inertia–gravity waves recently observed in experiments of WHR, followed by the conclusions and discussion in § 6.

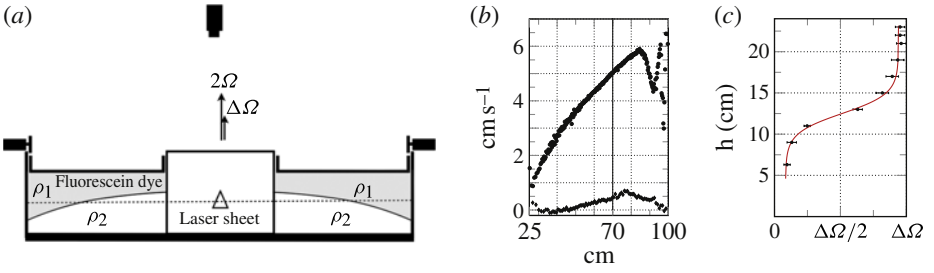

FIGURE 1. (Colour online available at journals.cambridge.org/flm) Sketch of the experimental setup (*a*) and typical measurements (*b*,*c*) of the azimuthal velocity with (*b*) its radial profile in the upper and lower layers, represented respectively by the upper and lower profiles, and (*c*) its vertical profile (maximum value). The vertical line in (*b*) indicates the approximate position of the frontal visualization and observation of the instabilities.

Exp.	H (cm)	g' (cm s^{-2})	Ω (rad s^{-1})	$\Delta\Omega$ (rad s^{-1})
A	13.5	5.80	0.030 → 0.498	0.104
B	13.5	5.49	0.025 → 0.498	0.056
C	13.5	6.67	0.030 → 0.500	0.073
D	13.5	6.68	0.040 → 0.500	0.125
E	11.0	5.59	0.040 → 0.500	0.125
F	13.5	6.18	0.050 → 0.278	0.146
G	13.4	6.00	0.108	0.105
H	13.6	4.00	0.049	0.100
I	13.2	6.00	0.098	0.082–0.125–0.165
J	13.5	4.70	0.118	0.125–0.094–0.073

TABLE 1. Experimental parameters within experiments A–F, Ω increasing with time, and Ω constant in experiments G–J. In experiments I and J, $\Delta\Omega$ was increased with the indicated steps.

2. Experimental setup and flow parameters

The experiments are conducted in an annulus of $R_1 = 100$ cm outer- and $R_2 = 25$ cm inner-radius tank of 40 cm working depth (see figure 1*a*), filled with a stable two-layer salt-stratified fluid, with equal depth layers of $H = 13.5$ cm. The fluid surface was covered with a rigid Perspex lid, which, in order to apply a vertical shear, was brought into rotation by three wheels, driven by stepper motors. The wheels were placed at equal distances at the rim of the lid (see figure 1*a*) and care was taken to minimize the disk perturbation, which was less than 5 mm in vertical amplitude during rotation. The tank was filled while rotating at a low rotation rate, Ω, of typically 0.05 rad s^{-1}. At $t = 0$ s, the rotation rate was slowly increased with an acceleration of 2.5×10^{-5} rad s^{-2}, while the annular disk at the surface was started to rotate cyclonically with a constant rotation, $\Delta\Omega$, chosen in the range between 0.1 and 0.4 rad s^{-1} (see table 1). For a final rotation speed of 0.5 rad s^{-1}, the experiment could take 2–3 h. In the course of an experiment, the two-layer stratification remained intact and, apart from the final irregular flow stage, relatively little mixing occurred between the two layers.

To visualize the flow, fluorescent dye was dissolved in the top layer, and illuminated by a horizontal laser sheet that intersected the inclined front at mid depth. In some

experiments a vertical light sheet visualized a radial section and allowed us to visualize the mixing between the two layers, and the thickening as well as the slope of the interface. The flow evolution was recorded with a frequency of 1 Hz with two 12-bit Dalsa cameras with a top-view camera mounted with a fish-eye lens, for which the deformation was corrected in the data processing. For each experiment, the values of F and d were plotted in a single graph (see figure 3) and the different regimes were determined qualitatively by scrutinizing the evolution of the front from the recordings. In order to double check the observed modes, experiments for a fixed background rotation (G, H) and for several consecutively increased disk rotations (I, J) were conducted (see table 1).

The experiments are controlled by four non-dimensional parameters: the Rossby number defined below, the rotational Froude number, $F = (4\Omega^2 L^2)/(g'H)$ (or Burger number $Bu = 1/F$), where the reduced gravity $g' = 2g(\rho_2 - \rho_1)/(\rho_2 + \rho_1)$ and $L = (R_2 - R_1)$, and the dissipation number, $d = \sqrt{(\nu\Omega)}/(H\Delta\Omega)$, determined by the ratio of the typical forcing time scale $1/\Delta\Omega$ and the Ekman spin-up time $\tau_{su} = H/\sqrt{\nu\Omega}$. The fourth number is the aspect ratio, H/L, which was kept constant at 0.18. The reduced gravity, g', was kept almost constant and close to the one used in WHR ($g' = 0.06$ m s^{-2}, see table 1).

For stable flows obtained for relatively slow disk speeds, horizontal velocity fields were measured at different heights in the two layers by means of particle image velocimetry (PIV). Typical profiles of the azimuthal velocity along the radius and height are, respectively, shown in figure 1(*b*,*c*). In the region of interest, the azimuthal velocity increases linearly with radius. For a disk rotation speed of $\Delta\Omega$, the rotation ratio between the upper and lower layers was found to be $\approx 0.9\Delta\Omega$ and $\approx 0.1\Delta\Omega$, compared to the 0.25–0.75 calculated from potential–vorticity conservation (Hart 1972) for two immiscible fluid layers. These different values are due to the larger interface thickness. In coherence with Gula *et al.* (2009*b*) and WHR, the Rossby number is defined as $Ro = \Delta\Omega/(2\Omega)$. With increasing background rotation, the Rossby number varied between $O(1)$ at the beginning and $O(0.1)$ at the end of an experiment. Since the Rossby number was in the range $0.06 < Ro < 1.5$, and the aspect ratio small, generally $(RoH/L)^2 \ll 1$ so that the hydrostatic approximation applies (see e.g. Hart 1979). Since $H/L = 0.18$ and the flow is forced in the horizontal direction, the shallow-water approximation is valid to leading order. Ageostrophic effects are therefore mainly present when the Rossby number is not small.

3. Frontal instabilities

With the accelerating background rotation, and corresponding increase in Froude and dissipation numbers, the following sequence of instability regimes is observed (see figure 2): axisymmetric flow (AX), Rossby–Kelvin instability (RK), baroclinic instability (BI) and eventually a flow with irregular baroclinic waves (IW). For small background rotation, an axisymmetric front is observed (see figure 2*a*). Small-scale waves appeared either on the entire front (figure 2*b*) or locally due to variations in the shear-layer and interface thicknesses (see figure 2*c*,*d*). With increasing background rotation, large-scale wave modes developed whereas the small-scale perturbations decreased in activity (figure 2*a–f*). The large-scale modes saturated at a low amplitude, resulting in a relatively modest deformation of the front (figures 2*a–c* and 4*a–f*). This instability, which we will refer to below as the RK instability (see figure 4*a–f*), continued to exist during the early stages of baroclinic instability. When increasing the

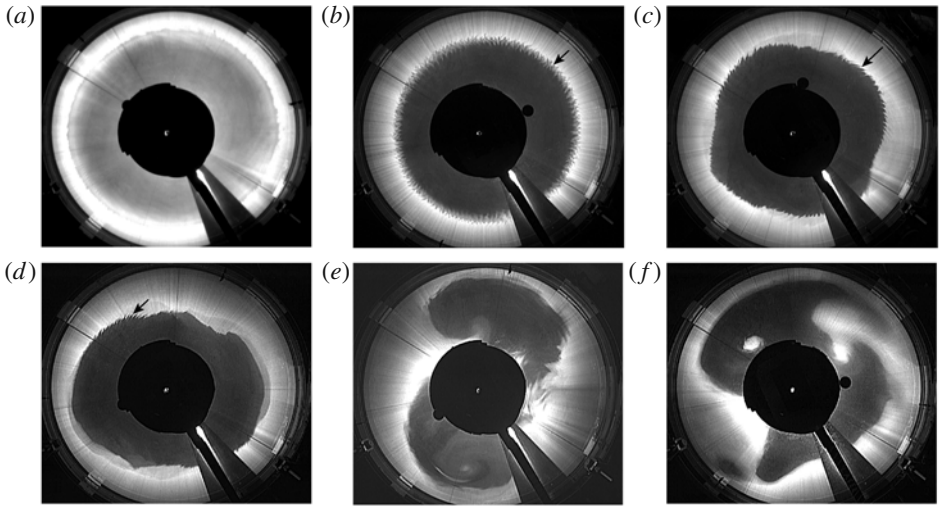

FIGURE 2. Series of top-view images showing the typical flow evolution, here for experiment A, with (*a*) $Ro = 0.95, Bu = 1.2, d = 0.017$; (*b*) $Ro = 0.72, Bu = 0.70, d = 0.019$; (*c*) $Ro = 0.46, Bu = 0.28, d = 0.024$; (*d*) $Ro = 0.34, Bu = 0.16, d = 0.028$; (*e*) $Ro = 0.32, Bu = 0.14, d = 0.029$ and (*f*) $Ro = 0.14, Bu = 0.028, d = 0.043$. Arrows point at examples of short scale waves (see discussion of § 5).

Froude number to values between 3 and 5, baroclinic modes 1 and 2 appeared to be dominant and continued to grow until the rim of the tank was reached (figure 2*d–f*).

In the logarithmic plot of figure 3, the values of the Froude number, F, and dissipation number, d, are represented for each experiment (straight black lines). The dotted and drawn lines between individual points separate the instability regimes. The RK instability appears after the axisymmetric regime with modes 1, 2 or 3 for low Froude numbers whereas for higher Froude numbers the mode increases up to 8. Since multiple modes often coexisted and made a single-mode observation difficult, regions of modes are indicated in figure 3.

At the left, the grey lines show the different regimes observed by WHR for an immiscible fluid interface. The lower dashed black line separates the Kelvin–Helmholtz regime from the stable regime and approximately adjoins the separation line for KH instability found by WHR. The baroclinic unstable regime sets in slightly earlier than the observations of WHR and the prediction according to the quasi-geostrophic theory for a two-layer theory of Hart (1972) (grey dashed line). The irregular regime (IW) in the present experiments corresponds to the regime called mixed irregular waves (MIW) in WHR. In this regime, the front changes rapidly but, probably due to the diffused interface, no small-scale interfacial perturbations were observed.

4. Rossby–Kelvin instability

Figure 5 shows the diagram of figure 3 in (Bu, Ro) space showing a comparison of the experimentally found modes with the numerical results obtained with the collocation code of Gula *et al.* (2009*b*) with instead of a rigid body rotation an azimuthal velocity field such as shown in figure 1(*b*). The lower line in figure 3 delimits the stable region, whereas above the upper grey line outcropping may

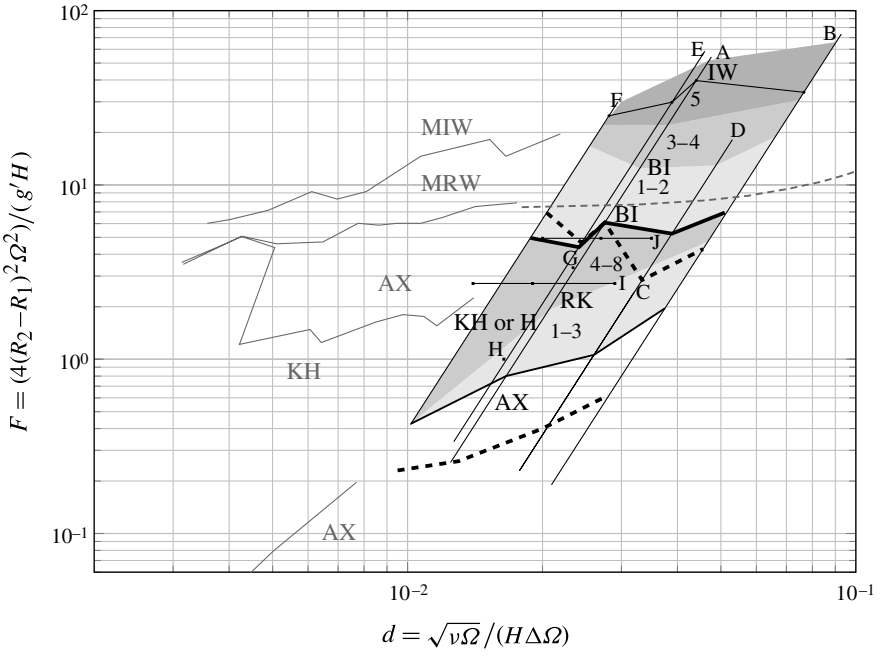

FIGURE 3. Regime diagram F–d. The inclined straight black lines correspond to experimental runs A–F, i.e. increasing background rotation, and single points constant background rotation (runs G–J) (see table 1). In the area delimited by thick dashed-lines, Kelvin–Helmholtz or Hölmböe (KH or H) instability occurs; the large-scale instability regimes (AX, RK, BI and IW) are delimited with lines, with BI starting above the bold black line. The grey zones indicate the different observed modes. Grey lines (left) represent adjoining results of Williams *et al.* (2005), with regimes: (AX) axisymmetric flow, (KH) Kelvin–Helmholtz instability, (MWR) mixed regular Waves and (MIW) mixed irregular waves. The grey dashed curve (right) represents the quasi-geostrophic neutral curve for baroclinic instability of Hart (1972).

be expected in addition to baroclinic instability. However, outcropping occurred intermittently because of nonlinear flow features such as amplitude vacillation, which, since it is beyond the scope of the present paper, is not considered here. In the RK-unstable region, the experimental results agree well with the numerical results for wavenumbers 5 and 6 (see figure 4) and globally show a similar trend with decreasing *Bu* number. In the regime (BI) there is good agreement with the numerical results and also the separation between the BI and the RK regimes is marked by a sudden decrease in wavenumber (see figure 5). However, the RK-instability region expands over a much wider range of *Ro* numbers. This difference and also the difference in the KH region may be explained by the high degree of idealization of the numerical model, i.e. a sharp density and shear-layer interface instead of a continuous density and shear-layer interface.

For each experiment, a space–time (or Hovmöller) diagram of the position of the front was established from the variation of the front position at each instant, $r_{front}(\theta, t)$ (with θ the azimuthal position in the tank and time t, see figure 6*a*). The grey value represents the wave displacement. The inclined grey areas indicate the motion of a crest (white) or trough (dark) and provide a measurement of the phase speed, c (see lines in figure 6*a*). The thus obtained non-dimensional phase speed, $c/2\Omega$, is presented

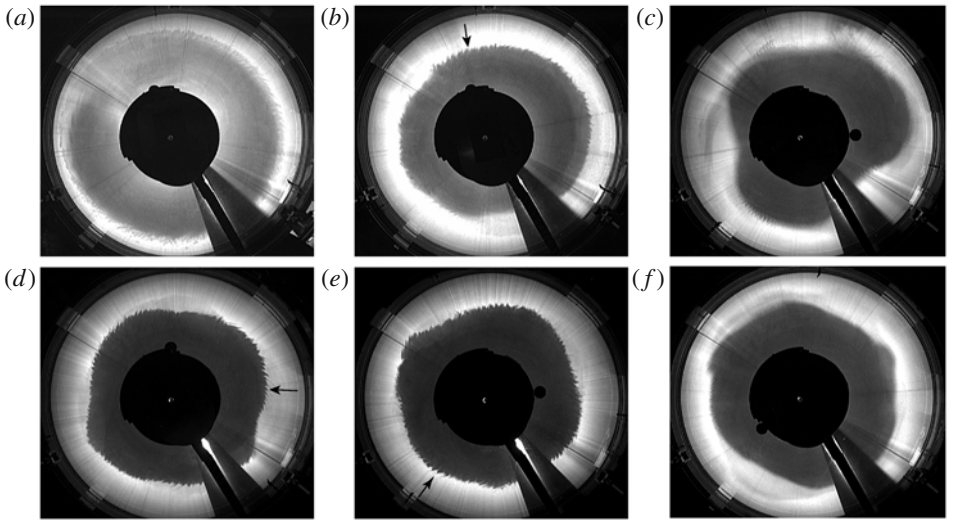

FIGURE 4. Observed modes of the RK instability with modes (*a*) 1, $Ro = 1.67$, $Bu = 1.99$, $d = 0.014$; (*b*) 1 and 2, $Ro = 0.94$, $Bu = 0.63$, $d = 0.019$; (*c*) 1 and 3, $Ro = 0.34$, $Bu = 0.50$, $d = 0.038$; (*d*) 4, $Ro = 0.46$, $Bu = 0.28$, $d = 0.024$ (*e*) 5, $Ro = 0.49$, $Bu = 0.32$, $d = 0.023$ and (*f*) 6, $Ro = 0.22$, $Bu = 0.21$, $d = 0.047$. The modes were observed in different experiments. Arrows point at examples of short scale waves (see discussion of § 5).

in figure 6(*b*) against the observed mode for the experiments G and I. For identical *Ro* and *Bu* numbers as in experiment G, the phase speed has been calculated numerically. For experiment I, the initial parameters were close to experiment G (see table 1). Both experimental results show good agreement with the numerical values for the RK modes as well as for the baroclinic modes, and therefore support the observation of the RK instability.

5. Short-scale waves

The small-scale waves are observed to have similar wavelengths in all regimes and have the same signature. Figures 2(*b*,*c*) and 4(*b*,*d*,*e*) show small-scale waves on top of the RK modes, and figure 2(*d*,*e*) on a baroclinic mode 2 (see arrows). They are typically of a wavelength of the order of the interface thickness, i.e. 3–6 cm, occur in regions with the largest shear and are cusp shaped. Their wave crests are observed to remain cusped shaped during the flow evolution and no Kelvin–Helmholtz billows developed (see figures 2 and 4). From space–time diagrams such as shown in figure 7(*a*), the phase speed is measured and was approximately constant with respect to the rotating frame of reference, i.e. they propagate in the retrograde direction with respect to the mean flow with a (dimensional) phase speed $-\Delta\Omega/2$. By contrast, Kelvin–Helmholtz billows are advected with the mean flow, as observed in some experiments, and propagate approximately with speed $\Delta\Omega/2$ with respect to the rotating frame of reference. These observations strongly suggest that these waves are in many cases due to the Hölmböe instability, as observed by Lawrence, Browand & Redekopp (1991).

In immiscible two-layer fluids in a smaller setup, short-scale waves have also been observed by Lovegrove *et al.* (2000) and Williams *et al.* (2005). These waves were interpreted as being spontaneously emitted inertia–gravity waves associated with

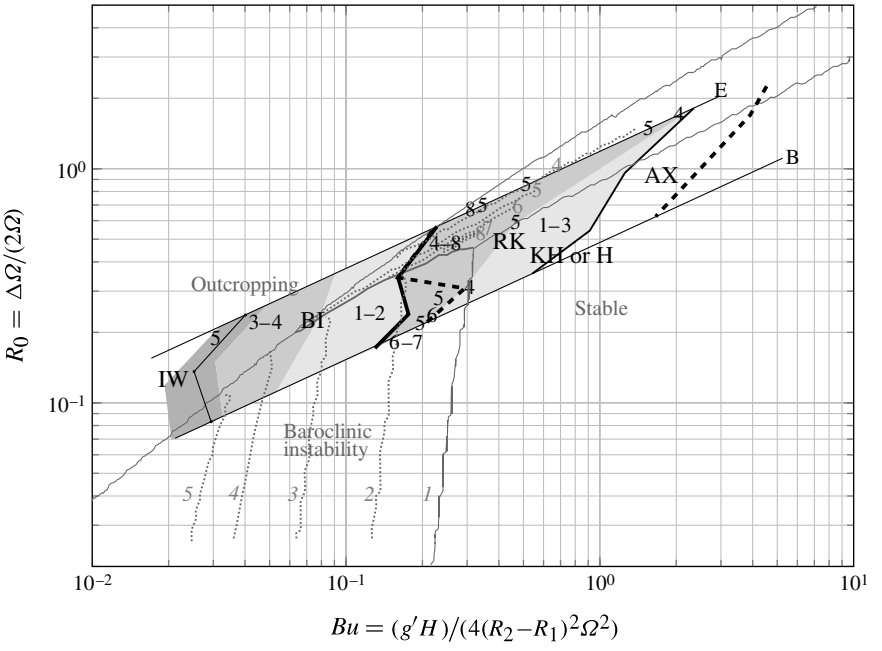

FIGURE 5. Comparison in *Ro–Bu* space between experimental results and numerical calculations (see text). Experimental results are represented as in figure 3 (with the experimental measurement region delimited with the lines of experiments E and B), the regimes (AX, RK, BI, IW) and the KH or H region, and the observed modes are indicated as in figure 3. In addition, experimentally observed modes are indicated by the numbers in black. The grey lines represent numerical results, with the lower line delimiting the stable region, and the upper line the limit to outcropping; the dotted lines represent the modes and the thick grey line the separation between baroclinic and RK instability.

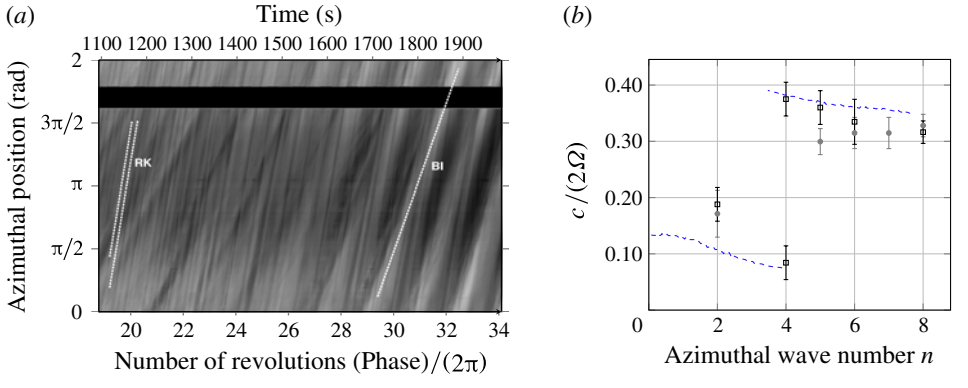

FIGURE 6. (Colour online) Space–time diagram for experiment G, with the white lines indicating the motion of the (BI and RK) instability (*a*) and thus obtained phase speeds (*b*) for experiments G and I. The dashed lines represent the numerical values for identical values of *Ro* and *Bu* as in experiment G, and the phase speeds obtained for experiments G and I represented respectively by filled and open symbols.

unbalanced flows (see Ford 1994 and McIntyre 2009). Hölmböe instability can grow for any value of the bulk Richardson number provided that the ratio of the thickness of

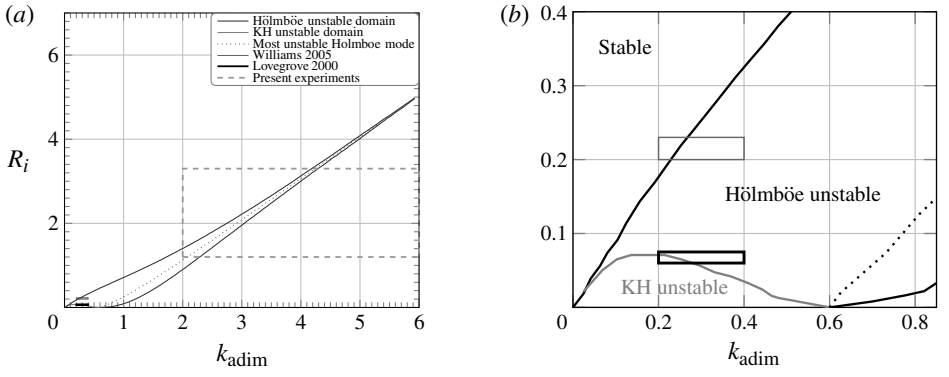

FIGURE 7. Diagram of Kelvin–Helmholtz and Hölmböe stabilities with the parameter regions considered in the present experiments and the ones reported in the literature (see legend) (*a*), and (*b*) a zoom on the region with Kelvin–Helmholtz instability (i.e. the region below the grey line) and the parameter regime considered in Lovegrove *et al.* (2000) and Williams *et al.* (2005).

the shear-layer interface to the density interface thickness is larger than 1. In practice, the Hölmböe instability has a relevant growth rate when this ratio exceeds a value of approximately 3 (see Carpenter, Balmforth & Lawrence 2010).

Figure 7(*a*) shows the stability diagram obtained with linear stability analysis of the Taylor–Goldstein equation for the case of a step-density profile and a piecewise-uniform velocity profile along the vertical direction (see e.g. Ortiz, Chomaz & Loiseleux 2002). Here, the definition of the bulk Richardson number is $Ri = (g'2\delta_s)/\Delta U^2$ based on the shear-layer thickness $2\delta_s$ and the dimensionless wavenumber along the abscissa $k\delta_s$, and $\Delta U = 0.8\Delta\Omega R$. The area covered by the present experimental data is large given the uncertainties in shear layer and density layer thicknesses and includes the possibility of Hölmböe waves as well as spontaneously emitted inertia–gravity waves.

In the experiments with immiscible fluids of Lovegrove *et al.* (2000) and Williams *et al.* (2005), the shear-layer thickness δ_s can be defined precisely by the Ekman-layer thickness at the interface, $\delta_e = \sqrt{\nu/\Omega}$. This thickness is much larger than the molecular thickness of the immiscible fluid interface. With this shear-layer thickness, the Richardson number follows the same definition as Williams *et al.* (2005). Accordingly, using figure 4 in Williams *et al.* (2005), which displays the evolution of R_i with the turntable rotation, we estimate the Richardson number and the wavenumber and superimpose the parameter areas on the stability diagram in figure 7(*b*). This shows that the observed small-scale perturbations can be due to Hölmböe instability, and less often due to Kelvin–Helmholtz instability. These results conjecture the above-described observations of Hölmböe waves.

6. Conclusions and discussion

These results report experimental observations of the RK instability investigated by Sakai (1989) and Gula *et al.* (2009*b*). For the instability regions BI and RK, reasonable agreement with the numerical results of Gula *et al.* (2009*b*) is obtained, whereas good agreement is obtained for the comparison with the phase speeds. The RK instability is found to saturate at a relatively small wave amplitude and occurs for

Burger numbers $0.15 \leqslant Bu \leqslant 2$ and moderate Ro number, i.e. approximately $0.2 > Ro > 2$. Baroclinic instability occurs for smaller Bu numbers, $Bu < 0.3$, i.e. earlier than predicted according to geostrophic theory and former experiments on frontal instability in immiscible fluids (WHR, Hart 1972).

Similar experiments for identical parameters as experiment F in a tank of 1 m-diameter without an internal cylinder showed that the RK instability conform with the here reported results. Therefore, the only pertinent difference between WHR and the present experiments is the immiscible fluid interface. Dissipative effects and the inhibition of the Rossby wave amplitude should be sufficient to suppress the RK instability and make its effect small. The RK instability favours intense small-scale instabilities near the outer boundary which are of the Kelvin–Helmholtz type (see Gula *et al.* 2009*a*, figure 16), as has been observed in the present experiments. At an immiscible fluid interface with different viscosity fluids, these vertical motions could be effectively dissipated and thus inhibit the growth rate of the instability. Indeed, the Reynolds number based on the flow width and velocity was of approximately 1000 or smaller in the experiments of e.g. Griffiths & Linden (1981) and Stegner, Bourouet-Aubertot & Pichon (2004). In WHR, and also Hart (1972), the Reynolds number is much larger than 2000 but the interfacial tension could more quickly dissipate the small-scale instabilities that occur during the transfer of kinetic energy to potential energy and damp the instability.

Frontal small-scale perturbations could in many cases be of Hölmböe type. Their appearance, wavelength and Richardson number in the present experiments and those of WHR support this hypothesis. To our knowledge, Hölmböe instability has not, or rarely been, observed in the context of frontal dynamics. For a density interface being shrouded by a relatively thick shear-layer interface, Hölmböe instability may appear for all Richardson numbers. One may therefore expect it to play an important role in frontal dynamics in many geophysical flows. For sufficiently high Reynolds numbers, the local shear may decrease the density interface thickness, but not necessarily the thickness of the shear-layer interface, and thus favour Hölmböe instability. In the light of the radiation of energy away from regions of high shear, the relevance of spontaneous emission of inertia–gravity waves remains to be further investigated, but waves generated by the Hölmböe instability could be a potential candidate that deserves more attention.

The authors acknowledge Adrien Capitaine for carrying out an initial set of experiments, S. Viboux and H. Didelle for improving the rotating platform that served for these experiments and support by ANR contract ‘FLOWINg’.

REFERENCES

CARPENTER, J. R., BALMFORTH, N. J. & LAWRENCE, G. A. 2010 Identifying unstable modes in stratified shear layers. *Phys. Fluids* **22**, 054104.

FLÓR, J.-B. 2007 Frontal instability, inertia-gravity wave radiation and vortex formation. 18 ème congres Francais de Mecanique. Url: http://devirevues.demo.inist.fr/handle/2042/15609.

FLÓR, J.-B., BUSH, J. W. M., BUSH, M. & UNGARISH, 2004 An experimental investigation of spin-up from rest of a stratified fluid. *Geophys. Fluid Dyn.* **98** (4), 277–296.

FORD, R. 1994 Gravity wave radiation from vortex trains in rotating shallow water. *J. Fluid Mech.* **281**, 81–118.

GRIFFITHS, R. W. & LINDEN, P. F. 1981 the stability of buoyancy-driven coastal currents. *Dyn. Atmos. Oceans* **5** (4), 281–306.

GULA, J., PLOUGONVEN, R. & ZEITLIN, V. 2009*a* Ageostrophic instabilities of fronts in a channel in a stratified rotating fluid. *J. Fluid Mech.* **627**, 485–507.

GULA, J., ZEITLIN, V. & PLOUGONVEN, R. 2009*b* Instabilities of two-layer shallow-water flows with vertical shear in the rotating annulus. *J. Fluid Mech.* **638**, 27–47.

HART, J. E. 1972 A laboratory study of baroclinic instability. *Geophys. Fluid Dyn.* **3**, 181–209.

HART, J. E. 1979 Finite amplitude baroclinic instability. *Annu. Rev. Fluid Mech.* **11**, 147–172.

LAWRENCE, G. A., BROWAND, F. K. & REDEKOPP, L. G. 1991 The stability of a sheared density interface. *Phys. Fluids* **3**, 2360–2370.

LOVEGROVE, A. F., READ, P. L. & RICHARDS, C. J. 2000 Generation of inertia–gravity waves in a baroclinically unstable fluid. *Q. J. R. Meteorol. Soc.* **126**, 3233–3254.

MCINTYRE, M. E. 2009 Spontaneous imbalance and hybrid vortex–gravity structures. *J. Atmos. Sci.* **66**, 1315–1326.

ORTIZ, S., CHOMAZ, J.-M. & LOISELEUX, T. 2002 Spatial Hölmböe instability. *Phys. Fluids* **14**, 2585–2597.

PEDLOSKY, J. 2001 *Geophysical Fluid Dynamics*, 2nd edn. Springer. p. 728.

SAKAI, S. 1989 Rossby–Kelvin instability: a new type of ageostrophic instability caused by a resonance between Rossby waves and gravity waves. *J. Fluid Mech.* **202**, 149–176.

SPENCE, G. S. M., FOSTER, M. R. & DAVIES, P. A. 1992 The transient response of a contained rotating stratified fluid to impulsively started surface forcing. *J. Fluid Mech.* **243**, 33–50.

STEGNER, A., BOUROUET-AUBERTOT, P. & PICHON, T. 2004 Nonlinear adjustment of density fronts. Part 1. The Rossby scenario and the experimental reality. *J. Fluid Mech.* **502** (1), 335–360.

WILLIAMS, P., HAINES, T. W. N. & READ, P. L. 2005 On the generation mechanisms of short-scale unbalanced modes in rotating two-layer flows with vertical shear. *J. Fluid Mech.* **528**, 1–22.